https://doi.org/10.5194/egusphere-2022-987
Preprint. Discussion started: 10 October 2022

Impact of permeability evolution in igneous sills on hydrothermal flow and hydrocarbon transport in volcanic sedimentary basins

Ole Rabbel[1*], Christophe Y. Galerne[2], Jörg Hasenclever[3], Olivier Galland[1], Karen Mair[1], Octavio Palma[4]

[1] NJORD, University of Oslo, P.O. 1048 Blindern, 0316 Oslo, Norway

[2] Faculty of Geosciences, University of Bremen, Klagenfurter Straße 2-4, 28359 Bremen, Germany

[3] Institute of Geophysics, Center for Earth System Research and Sustainability, University of Hamburg Bundesstrasse 55, 20146 Hamburg, Germany

[4] Facultad de Ciencias Naturales y Museo, Universidad de La Plata, Paseo del Bosque s/no - B1900FWA – La Plata, Argentina

*Corresponding author, e-mail: ole.rabbel@gmail.com

https://doi.org/10.5194/egusphere-2022-987
Preprint. Discussion started: 10 October 2022

Abstract:

Sill intrusions emplaced in organic-rich sedimentary rocks trigger the generation and migration of hydrocarbons in volcanic sedimentary basins. Based on seismic and geological observations, numerical modeling studies of hydrothermal flow around sills have shown that thermogenic methane is channeled towards the intrusion tip, where it rises to the surface in a hydrothermal vent. However, these models typically assume impermeable sills and ignore potential effects of permeability evolution in cooling sills, e.g., due to fracturing. To address this issue, we combine a geological field study of a volcanic basin (Neuquén Basin, Argentina) with hybrid FEM/FVM numerical modeling of hydrothermal flow around a sill, including hydrocarbon generation and transport. Our field observations show that graphitized bitumen veins and cooling joints filled with solid bitumen or fluidized shale are common within the studied sills. Raman spectroscopy indicates graphitization at temperatures between 350-500°C, evidencing fluid flow within the intrusions shortly after solidification. This finding motivates our modeling study, which investigates flow patterns around intrusions that become porous and permeable upon solidification. The results show three distinct flow phases affecting the transport of hydrocarbons generated in the contact aureole: (1) Contact-parallel flow toward the sill tip before solidification, (2) upon complete solidification, sudden vertical “flushing” of overpressured hydrocarbon-rich fluids from the lower contact aureole through the hot sill, and (3) slow rise of hydrocarbon-rich fluids above the sill center, and backward-downward flow near the sill tip. We conclude that permeability creation within cooling sills may be an important factor for hydrothermal flow and hydrocarbon transport in volcanic basins, as it considerably alters the fluid pressure configuration and flow patterns by dissipating overpressure below the sills. This could, for instance, lead to a reduced potential for hydrothermal venting.

https://doi.org/10.5194/egusphere-2022-987
Preprint. Discussion started: 10 October 2022

1 Introduction

Sill intrusions emplaced in sedimentary rocks strongly influence the generation and migration of hydrocarbons and greenhouse gases in volcanic sedimentary basins. If sill intrusions are emplaced in organic-rich strata, they trigger contact-metamorphic reactions (e.g., organic matter transformation), overpressure generation, and hydrothermal fluid flow in the surrounding strata (Einsele et al., 1980; Aarnes et al., 2012). Many recent studies of volcanic sedimentary basins investigate how such processes may cause the formation of hydrothermal vent complexes, which facilitate greenhouse gas release to the atmosphere and can thus drive global climate change (Svensen et al., 2004; Aarnes et al., 2010; Aarnes et al., 2012; Iyer et al., 2013; Iyer et al., 2017; Galerne and Hasenclever, 2019). Additionally, the same processes can be critical factors for hydrocarbon generation and migration in igneous petroleum systems containing sills emplaced within shale formations (Senger et al., 2017; Spacapan et al., 2020).

Hydrothermal flow in response to the intrusion of magma into sedimentary host rocks has been investigated for decades. The magmatic heat input leads to several temperature-dependent processes that promote strong fluid pressure increase, which drive fluid flow (Einsele et al., 1980; Delaney, 1982). These processes include for instance thermal fluid expansion, mineral dehydration, organic matter transformation into hydrocarbon generation, and pore space reduction due to mineral precipitation (Einsele et al., 1980; Delaney, 1982; Aarnes et al., 2010; Townsend, 2018). When the rate of overpressure generation is larger than flow-driven pressure dissipation, e.g. in low-permeable rocks like shale, hydraulic fractures form and locally enhance fluid flow and pressure release (Aarnes et al., 2012; Kobchenko et al., 2014; Panahi et al., 2018; Rabbel et al., 2020). This process may lead to explosive hydrothermal vents, which are present in several volcanic basins (Nermoen et al., 2010; Aarnes et al., 2012; Iyer et al., 2017).

Numerical models simulate these coupled processes to understand hydrothermal flow dynamics and the associated hydrocarbon migration (usually represented as methane carried in the hydrothermal fluids), typically in the context of vent formation around sills emplaced in organic-rich sediments. Such simulations assume that sills are impermeable and show that vents seem to preferentially form at the inclined tips of large “saucer-shaped” sills because this situation favours both fast fluid pressure build-up below the sills and focussed fluid

https://doi.org/10.5194/egusphere-2022-987
Preprint. Discussion started: 10 October 2022

migration towards the tips (Iyer et al., 2013, Iyer et al., 2017; Galerne and Hasenclever, 2019).

However, observations from several volcanic sedimentary basins indicate that the assumption of impermeable sills is not generally valid. Sills often host fracture networks including different fracture types. These form shortly after solidification of the magma and may include columnar cooling joints or fractures related to hydraulic fracturing during hydrothermalism (Senger et al. 2015, Witte et al. 2012, Rabbel et al., 2021). Multiple studies have provided evidence that such fracture networks may be open and can contain water (Chevallier et al., 2004) or hydrocarbons and act as fluid pathways or even fractured reservoirs (Mark et al., 2018; Schofield et al., 2020; Spacapan et al., 2020). However, it is currently unknown to which extent the generation of fractures during the cooling phase of sills affects hydrothermal flow and associated hydrocarbon migration in volcanic basins.

To address this issue, we present a geological case study from the northern Neuquén Basin, Argentina, combined with numerical hydrothermal simulations. The northern Neuquén Basin provides particularly well-documented examples of sills with extensive cooling joint networks emplaced in organic-rich shale because the fractured sills represent the main reservoirs in several commercially producing oil fields (Rodriguez Monreal et al., 2009; Witte et al., 2012; Spacapan et al., 2020). Additionally, numerical modeling and subsurface data demonstrate the strong thermal impact of intrusions on host rock maturation in these systems (Rodriguez Monreal et al., 2009; Spacapan et al., 2018). We first present geological evidence from outcropping sills to provide evidence for hydrocarbon transport through fractured sills in a hydrothermal environment. Our field observations motivate the implementation of numerical modelling to test the influence of cooling joint formation, i.e. permeable sills, on the hydrothermal flow patterns and hydrocarbon migration. We performed a parameter study, in which we test this effect for sills of varying thickness and emplacement depth. By integrating the simulation results with geological evidence, we show how permeable sills affect hydrothermal flow in volcanic sedimentary basins as well as the fate of hydrocarbons generated by contact metamorphism.

https://doi.org/10.5194/egusphere-2022-987
Preprint. Discussion started: 10 October 2022

2 Geological observations

2.1 Geological setting

The study area is located around the Río Grande Valley (RGV) in the northern Neuquén Basin, Argentina, about 100 km south of the town of Malargüe (Figure 1). The Neuquén Basin initially formed as a series of isolated half-grabens during the late Triassic to early Jurassic (Howell et al., 2005). During the middle Jurassic to early Cretaceous, these depocenters coalesced during thermal subsidence, forming a large shallow-marine basin. This phase included the deposition of the Vaca Muerta and Agrío formations, which comprise several hundreds of meters of calcareous, organic-rich shale and form two important source rock formations for presently exploited petroleum systems (Kietzmann et al., 2014). From the early Cretaceous, the basin developed into a foreland basin in response to the compressive tectonic regime of the Andean orogeny. This led to inversion of the Triassic normal faults and

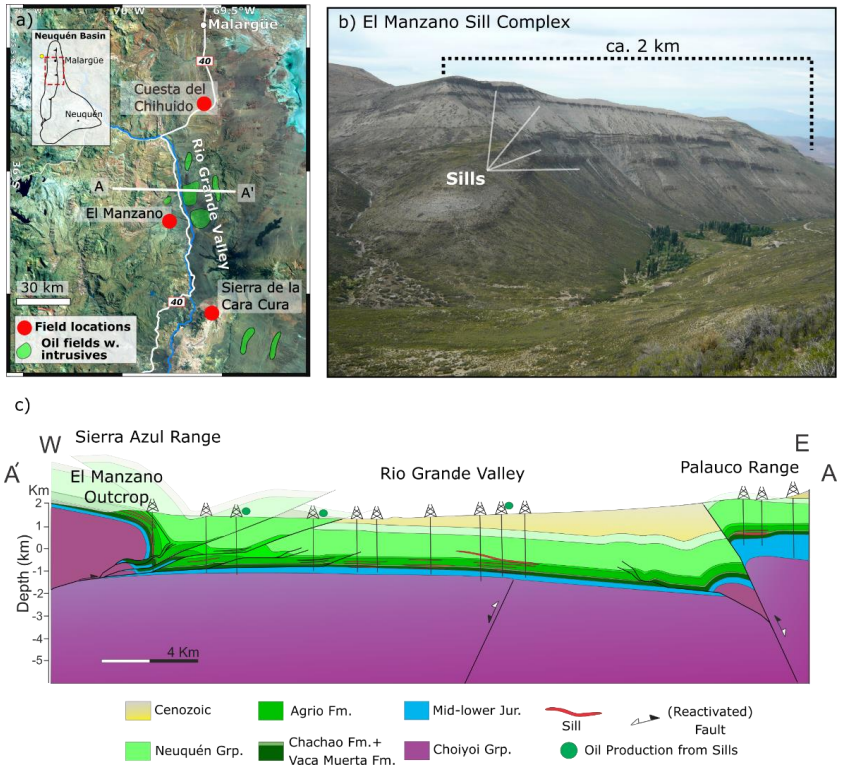

Figure 1. (a) Satellite image of the study area in the northern Neuquén Basin including field localities (red dots) and producing igneous petroleum systems (green areas). (b) View of the El Manzano sill complex outcrop in the Sierra Azul range (Photo: F. Soto). (c) E-W structural geological section illustrating the relation between subsurface and outcropping sill complexes (courtesy. J. B. Spacapan)

https://doi.org/10.5194/egusphere-2022-987
Preprint. Discussion started: 10 October 2022

generation of a series of fold-thrust belts along the western basin boundary (Manceda and Figueroa, 1995; Yagupsky et al., 2008).

In addition to tectonic deformation, the northern Neuquén Basin experienced intense magmatic activity that formed a series of volcanic plateaus and widespread magmatic intrusions within the sedimentary succession (Kay et al., 2006). In the study area, two main eruptive cycles, termed Molle and Huincán eruptive cycles, occurred in the late Oligocene-mid Miocene and the late Miocene-Pleistocene, respectively (Combina and Nullo, 2005). These events lead to the emplacement of extensive andesitic and basaltic sill complexes predominantly in the Vaca Muerta and Agrío Formations, but also in overlying gypsum and sandstone units (Spacapan et al., 2020).

In the RGV, heavily fractured sills emplaced in the Vaca Muerta and Agrío formations constitute the reservoirs in an actively producing igneous petroleum system (Schiuma, 1994; Witte et al., 2012). Spacapan et al. (2020) reported 2 to 27 m thick sills in these shale formations, but up to 54 m within shallower clastic sediments of RGV. Other studies from the northern Neuquén Basin report thick laccolith intrusions (>100 m) acting as reservoirs (Rodriguez Monreal et al., 2009). Spacapan et al. (2018) showed that the heat input provided by the sills matured the Vaca Muerta and Agrío shale formations, which otherwise show very low thermal maturity at burial depths of ca. 2-2.5 km. The established model for the formation of these igneous reservoirs includes that the intrusions developed interconnected cooling joint networks, which subsequently stored the generated hydrocarbons (Witte et al., 2012; Spacapan et al., 2020).

In addition to the subsurface sill complexes, thrust tectonics brought to surface exceptional outcrop analogues in the surrounding mountain ranges including the Sierra Azul, Sierra Cara Cura, and Cuesta del Chihuido (Figure 1). Several studies describe these localities, which offer easy access to sills emplaced in the Vaca Muerta and Agrio formations (Spacapan et al., 2017; Rabbel et al., 2018; Rabbel et al., 2021). Especially the km-scale outcrops at El Manzano (Figure 1b) and Sierra Cara Cura constitute direct analogues to the subsurface sill complexes of the RGV igneous petroleum system (Palma et al., 2019; Rabbel et al., 2021). These three field localities are ideal case studies to reveal the interactions between igneous intrusions and the petroleum system.

https://doi.org/10.5194/egusphere-2022-987
Preprint. Discussion started: 10 October 2022

2.2 Field methods

The fieldwork conducted for this study aims to document evidence of hydrothermal flow and hydrocarbon transport related to permeable intrusions in the study area. During three field campaigns, we collected an extensive dataset at the outcrops in El Manzano, Sierra de la Cara Cura, and Cuesta del Chihuido (Figure 1). We gathered ground-based and drone digital photographs to document outcrop observations. Additionally, we collected over 100 rock samples from the intrusions, surrounding shale as well as various types of veins for geochemical analyses. Here, we focus on presenting field evidence for hydrothermal flow of hydrocarbon-bearing fluids both around and within the sills, which then motivates the numerical study. Note that a more comprehensive description of the field study is presented by Rabbel et al. (2021).

2.3 Observations of hydrocarbons inside and around sills

Outcropping sills in all three localities feature solid bitumen and black shale inside the fracture network of the sills. At Cuesta del Chihuido, both the side and roof of thin sills are exposed, and the side view reveals upwelling dykelets of black shale (Vaca Muerta Formation) entering the sill from the bottom contact (Figure 2a). The top view of the same sill shows the entire polygonal cooling joint network with a black fill of the same material (Figure 2b). Brecciated igneous material often surrounds the dykelets where they enter the intrusion.

The larger sills at El Manzano (Sierra Azul) and Sierra Cara Cura also show widespread bitumen in the fracture network of the sills, but at a much larger scale (Figure 3). We observe arrays of 1-up to 50 cm thick and >10 m high bitumen dykes or veins (Figure 3a). Here, the bitumen dyke cuts across the contact aureole and enters the sill intrusion. We find exposures of similar structures where the sill interior is accessible (Figure 3b). The sill appears heavily fractured in addition to preexisting cooling joints, and solid bitumen or calcite fill nearly all fractures. On closer inspection, the bituminous material in these veins has a shiny and fibrous texture.

At an exposed sill tip at El Manzano, we also observe that thick bitumen veins appear to be concentrated along the tip contact, where they mutually cross-cut with calcite veins of at least similar thicknesses (Figure 3c,d). These calcite veins have cm-scale pores, which occasionally

https://doi.org/10.5194/egusphere-2022-987
Preprint. Discussion started: 10 October 2022

contain solid bitumen themselves and release a strong hydrocarbon smell when the vein is broken up.

2.4 Bitumen characterization

The fibrous texture of the observed bitumen within the sills is intriguing and suggests that it partly experienced graphitization, i.e. it is much higher-grade bituminous material than that described in the Neuquén basin by Cobbold et al. (1999) and Zanella et al. (2015).

In the field, we tested this hypothesis by measuring the resistivity of the fibrous bitumen with a hand-held multimeter. Graphitization of bitumen significantly changes the electric resistivity of the material: amorphous solid bitumen is very resistive and used as an electric insulator in industry applications (Hays et al., 1967), while graphite is an excellent conductor. Qualitative on-site resistivity measurements showed that the fibrous bitumen conducts electric currents well, i.e., within the detection limit of a standard multimeter, suggesting significant graphitization.

In addition, we applied Raman spectroscopy to better constrain the nature of the solid bitumen and its thermal history. Raman spectroscopy provides positions and relative intensities of spectral peaks characterizing carbonaceous materials like bitumen, including D ("disorder") and G ("graphite") peaks at 1345 cm^{-1} and 1585 cm^{-1}, respectively (Potgieter-Vermaak et al., 2011; Rantitsch et al., 2016). The shape of the spectra and the D/G peak and area ratios allow classification of high-grade alteration of the bitumen to anthracite or (semi-)graphite and may serve as a geothermometer for high-temperature regimes (Beyssac et al., 2002; Rantitsch et al., 2016). Due to the high temperatures within and around igneous intrusions, we expect this method to indicate the degree of thermal alteration and thus temperatures that the hydrocarbons experienced. Since Raman spectra can show varying absolute intensities, we normalized each spectrum to the intensity of the respective G peak (I_G) for visualization purposes.

https://doi.org/10.5194/egusphere-2022-987
Preprint. Discussion started: 10 October 2022

201

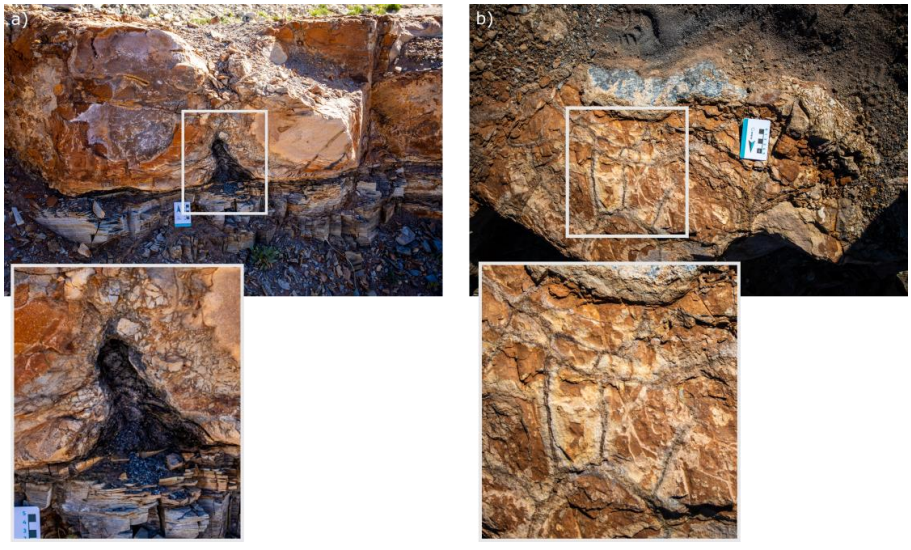

Figure 2. Field observations of upwelling dykelets of liquefied shale and bitumen entering the cooling joint network of a thin sill at Cuesta del Chihuido (ca. 30 cm thick). (a) Side view showing the sediment-intrusion contact and dyke (Photo: D. Michelon), (b) top view demonstrating black bituminous fill in the polygonal cooling joints.

202

203 Raman spectrograms of the sampled bitumen veins show very clearly developed G and D1
204 peaks and I_{D1}/I_G ratios of 0.6 and 0.9, respectively. The D3 band between the peaks is nearly
205 absent in the sample from Sierra de la Cara Cura, while it is visible at low intensity in the
206 presented sample from El Manzano (Figure 4).

https://doi.org/10.5194/egusphere-2022-987
Preprint. Discussion started: 10 October 2022

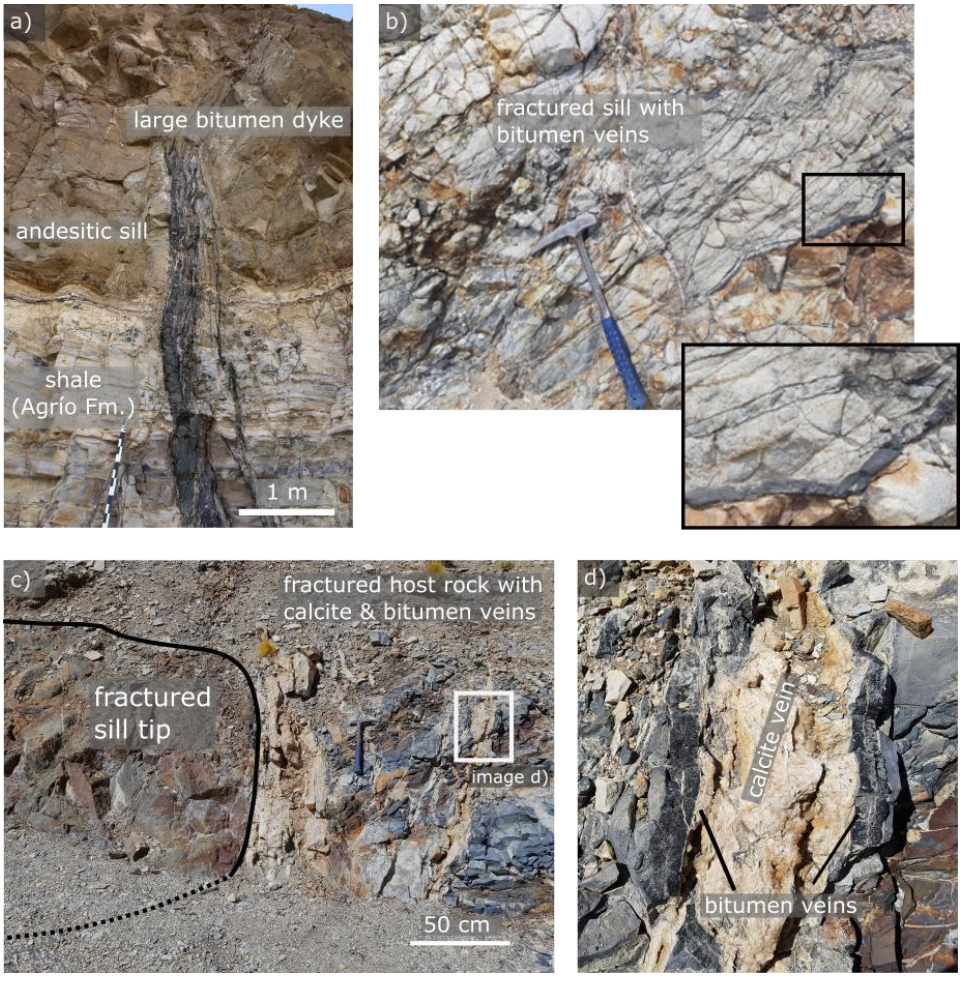

Figure 3. Examples of dykes or veins of solid bitumen associated the sill intrusions. (a) Bitumen dyke at El Manzano of >10 m height and up to 0.5 m thickness originating in the aureole of Agrío Fm. and entering the sill through the bottom contact. (b) Fractured zone inside a sill at Sierra de la Cara Cura exhibiting many cm-scale veins of solid bitumen. (c, d) Exposed sill tip at El Manzano showing high concentration of fibrous bitumen and calcite veins in the contact in front of the tip.

2.5 Composition and thermal implications of bitumen samples

We compare our Raman results with those measured in carbonaceous material from several studies, where increased graphitization and metamorphism lead to well-developed, narrow graphite (G) and disordered carbon (D1) peaks, weak or absent D3 bands, and I_G/I_D peak ratios of <1 (Beyssac et al., 2002; Kwiecinska et al., 2010; Rantitsch et al., 2016). Although we did not perform quantification via peak-fitting, a qualitative comparison of our results with highly metamorphosed sediments presented by Beyssac et al. (2002, Fig. 6 and 11

https://doi.org/10.5194/egusphere-2022-987
Preprint. Discussion started: 10 October 2022

therein) leads to estimated temperatures of 350-500°C for our samples (Figure 4). Hydrothermal graphitization can occur along intrusion-sediment contacts at relatively shallow crustal levels and requires temperatures of >= 400°C (Buseck and Beyssac, 2014). Hydraulic fracturing focuses the flow of hydrothermal fluids oversaturated with CH_4 and/or CO_2 from which crystalline graphite may precipitate (Rumble, 2014). This fits well with the observations that the bitumen dykes in our study area consist of pure, often crystalline graphitic material and occupy fractured zones in the aureole, around the tip, or within the sills themselves (Figure 3). In a previous summary of fracture types present in the sills of the study area, Rabbel et al. (2021) interpreted these features as hydraulic fractures. Thus, evidence from graphitized bitumen in the fractures in the aureole and the sills themselves points to hydrocarbon transport in a high-pressure, high-temperature environment in which at least part of the mobilized carbon transforms to graphitic carbonaceous material.

Our field and sample results strongly suggest that significant volumes of hydrocarbons circulated through the sills when the temperature at their margins was 350-500°C. The temperature was thus likely much higher in the interior of the sills. We infer that hydrothermal flow also occurred along cooling fractures within the sill, i.e., the sill developed some permeability while still hot (cf. Figure 2). This interpretation challenges the assumptions of previous models of hydrothermal circulation around cooling sills, in which the sills remain impermeable during cooling (Aarnes et al., 2012; Iyer et al., 2017, Galerne & Hasenclever, 2019). To which extent permeability creation within hot sills affects hydrothermal flow and the associated hydrocarbon transport around sills is not known. In the following section, we therefore present numerical simulations to test the effects of permeability increase associated with fracturing within the sills on hydrothermal circulations, and how this affects hydrothermal transport of hydrocarbons around sills.

https://doi.org/10.5194/egusphere-2022-987
Preprint. Discussion started: 10 October 2022

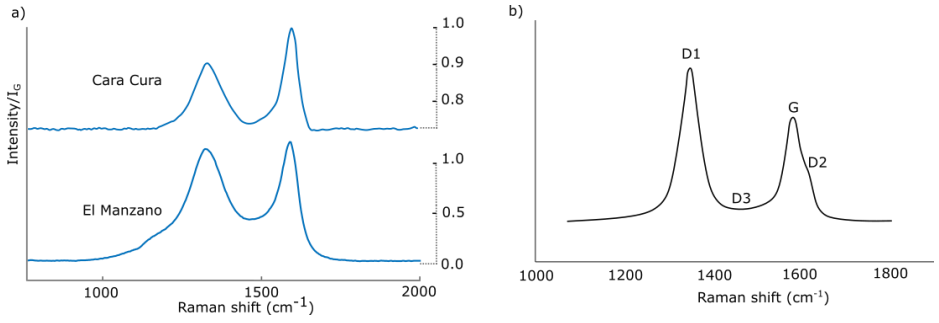

Figure 4. (a) Raman spectra from two bitumen vein samples at Sierra de la Cara Cura and El Manzano, respectively. Both samples include well-developed and narrow graphite and disordered carbon (G, D1) peaks as well as weak or absent D3 band. (b) Reference Raman spectrum to illustrate spectra decomposition of carbonaceous material after Beyssac et al. (2002).

3 Numerical Simulations

3.1 Model description

We employ the two-dimensional (2D) finite element model of Galerne and Hasenclever (2019), who applied it to quantify degassing through sill-related hydrothermal vents. As this complex model is presented in detail in Galerne and Hasenclever (2019), we will limit our discussion to the main features and point out the key adjustments for this study. In short, the model simulates hydrothermal flow around a cooling sill but is also coupled to a model for the heat-driven chemical transformation of organic matter into hydrocarbons (represented by methane). This allows us to investigate not only hydrothermal circulation around sills as such but also how this affects the transport of the hydrocarbons generated in the aureole.

The model considers single-phase hydrothermal flow of a compressible fluid in a porous medium following Darcy's law. Temperature calculations comprise heat diffusion, heat advection and heat sources/sinks related to latent heat of magma crystallization, dehydration, thermal cracking of organic matter as well as internal fluid friction and pressure-volume work. Fluid density varies with temperature and pressure according to the equation of state of pure water. The pore pressure equation also contains source terms representing fluid release due to temperature-dependent, irreversible contact metamorphic reactions, including (i) organic matter transformation into methane and (ii) clay mineral dehydration.

To calculate organic matter transformation to methane, the model uses the EASY%Ro method (Sweeney and Burnham, 1990), which quantifies the converted fraction of organic

https://doi.org/10.5194/egusphere-2022-987
Preprint. Discussion started: 10 October 2022

matter and thermal maturity through vitrinite reflectance *Ro*. We monitor transport and accumulation of the released methane due to hydrothermal flow using a finite volume advection scheme, but do not consider buoyancy effects resulting from the addition of methane to the pore fluid. Clay mineral dehydration follows the maximum storable weight fraction of water in the stable mineral assemblage at a given temperature, which is predicted by phase equilibria (Connolly, 2009). This process not only produces additional pore fluid, but also causes a permanent porosity increase in the affected host rock to ensure mass conservation of rock and fluid. Note here that while the model uses the properties of methane, the results can be used to understand transport of (light) hydrocarbons around sills in general. We thus use "methane" and "hydrocarbons" interchangeably in the context of this study.

The model provides time series of the 2D fields of all relevant rock properties in the model domain and physical quantities related to metamorphism and hydrothermal flow. Since we investigate the impact of permeable sills on the fluid and hydrocarbon circulation, our analysis focuses on visualization of the flow fields and methane accumulation during cooling.

3.2 Adjustments for this study

We adjusted two aspects of the original model to honor geological observations in the study area. First, we limit the permeability increase in the host rock due to rock fracturing to tensile hydraulic fracturing, but do not consider shear failure. At sufficiently high pore fluid overpressure, i.e., if pore pressure exceeds the sum of lithostatic stress and tensile strength, we assume that hydrofracturing occurs and increases permeability. Here, we consider hydrofracturing of the aureole only, not within sill.

Second, we approximate the process of joint formation within the sill through a linear porosity-permeability increase that is a function of temperature. Geological observations from the Neuquén Basin suggest that an open (cooling) joint network developed in the sills through which hydrocarbon-bearing hydrothermal fluids entered the sill while it was still hot enough to cause graphitization (Figure 2, Figure 3, Figure 4). Cooling joints form as a result of bulk volume reduction of the cooling and crystallizing magma, which induces thermal stresses that lead to the formation of a cooling joint network, creating primary porosity and permeability inside the intrusion (e.g., Petford, 2003; Hetényi et al., 2012). The overall pore-space gained in the model is set to equate 8% volume loss, occurring during the transition from a melted to crystallized magma (between the liquidus and solidus temperature), based on reported fracture porosities from fractured sill reservoirs in the study area (Witte et al., 2012; Spacapan et al., 2020). To be

https://doi.org/10.5194/egusphere-2022-987
Preprint. Discussion started: 10 October 2022

consistent with the crystal-mush model described by Marsh (2002), the onset of the pore opening should be when 50-55% of the magma has crystallized. Here we take a value of 1000°C as the onset of the brittle-ductile-transition (BDT) temperature. Using a linearized, temperature-dependent definition of the melt fraction, $(T-T_S)/(T_L-T_S)$, with T_L = 1100°C and T_S = 900°C being liquidus and solidus temperatures, resp., the set value for the BDT in our simulations implies that cooling joint creation starts when, at any distance from the sill margins, 50% of the sill has crystallized.

Note that in this way, we limit the model's representation of fracturing in the sill to cooling joints and thus perform a strong simplification compared to the complex interplay of fracturing mechanisms observed in the field (cf. section 3 and Rabbel et al, 2021). However, the goal is to study the general impact of permeable sills on hydrothermal flow and the associated hydrocarbon transport, which should be possible even with this limitation.

3.3 Modeling setup

We designed our modeling study to approximate the conditions of our study area, although we simplified the setup for the sake of a well-constrained parameter study. Figure 5 and Table 1 show the model setup and the list of important model parameters, respectively.

The model domain extends from the surface to 500 m below the emplacement depth of the sill. We assume instantaneous sill emplacement at 1100°C, corresponding to the inferred liquidus temperatures of andesitic magma in the study area (Spacapan et al., 2018). Since flow patterns around idealized flat sills tend to be symmetric, we limited our studies to a 500 m long "half", flat sill intrusion (Figure 5a). This allows to evaluate processes around and within the sill at very high resolution of 0.5 m. The left and right boundaries are insulating and impermeable, and we calibrated the temperature at the bottom boundary to create a geothermal gradient of around 30°C/km. The top boundary mimics the behaviour of the sea floor with free in- and outflow. Otherwise, initial conditions consider no basin history such as uplift and erosion, and no pre-existing thermal maturation before sill emplacement. We justify this by low background maturity values reported in the study area (Spacapan et al., 2018; Palma et al., 2019; Rabbel et al., 2021)

https://doi.org/10.5194/egusphere-2022-987
Preprint. Discussion started: 10 October 2022

322 For the sediments, we chose a homogenous material with 5% TOC and ca. 5 weight percent
323 bound water, as well as exponential decay of porosity with depth (Figure 5b). Permeability is
324 porosity-dependent and follows a Kozeny-Carman relationship. All values are calibrated to
325 local organic-rich shale, i.e. low porosity and low permeability rocks (Figure 5b). We chose
326 the specific values to match properties of Agrio and Vaca Muerta formations at 2-3 km depth

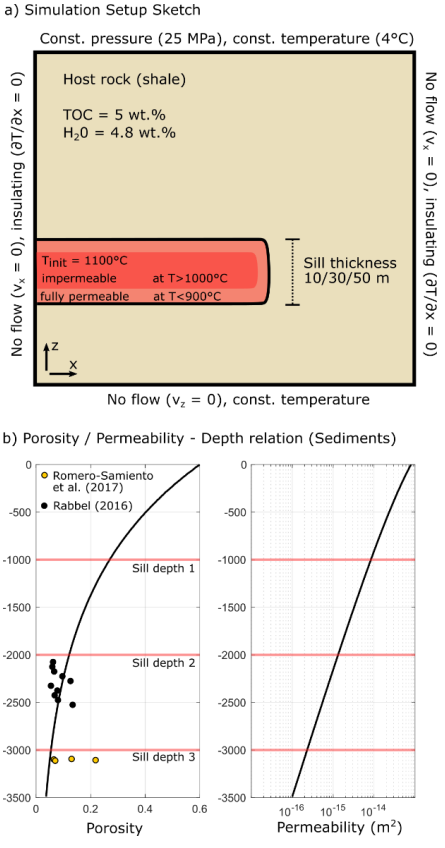

Figure 5. Illustration of the numerical modelling setup. (a) Sill geometry, boundary and initial conditions (not to scale). (b) Left: Porosity-depth relationship calibrated using reported data from the Vaca Muerta formation from various depths (Rabbel 2017, Romero-Samiento et al. 2017). Right: Permeability as a function of depth-

327 in the northern Neuquén Basin, which corresponds to emplacement depths for the igneous
328 petroleum systems present in both subsurface and outcrop.

329
330
331
332

https://doi.org/10.5194/egusphere-2022-987
Preprint. Discussion started: 10 October 2022

3.4 Parameter sensitivity study

In total, we ran 27 simulations to investigate the effects of

- porosity and permeability generation within sills
- emplacement depth, i.e., sediment permeability and porosity (1, 2, 3 km)
- intrusion thickness (10, 30, 50 m)

We first conduct a series of reference setups including permanently impermeable sills but allowing hydraulic fracturing of the host rock. All combinations of emplacement depth and sill thickness lead to a total set of 9 reference simulations. Subsequently, we use the same setups but activate temperature-dependent porosity and permeability generation for the sills.

Table 1. Material properties used for hydrothermal simulations

Fixed rock parameters	Value	Unit
Fluid Properties	Follow eqn. of state for pure water (IAPS-84)	
Magma / Sill Properties (representing andesite)		
Specific heat capacity[1,2]	900	J kg^{-1} K^{-1}
Latent heat of crystallization[1,2]	320	kJ/kg
Initial sill temperature[3,4]	1100	°C
Liquidus temperature[3]	1100	°C
Solidus temperature[4]	900	°C
Brittle-Ductile-Transition (permeability creation)	1000-900	°C
Permeability range in sill[4]	10-20 – 10-15	m^2
Sill thickness[4]	10, 30, 50	m
Magma density[2,6]	2830	kg/m^3
Thermal conductivity	2.51	W m^{-1} K^{-1}
Host Rock Properties (representing shale)		
Density[6]	2600	kg/m^3
Specific heat capacity[5]	960	J kg^{-1} K^{-1}
Thermal conductivity[5]	2.55	W m^{-1} K^{-1}
Porosity[6]	Ref fig	Ref fig
Permeability	Ref fig	Ref fig
Initial TOC[4]	0.05	1
Initial bound water content[2]	0.048	1
Tensile strength[7]	3	MPa

https://doi.org/10.5194/egusphere-2022-987
Preprint. Discussion started: 10 October 2022

Sources:
[1]Aarnes et al. (2010), [2] Galerne and Hasenclever (2019), [3] Stern et al. (1975) [4], Spacapan et al. (2018), [5]Angenheister et al. (1982), [6] Rabbel (2017), [7] Schön (2015)

3.5 Numerical Simulation: results

3.5.1 Impermeable sill: Flow focusing and methane plume

We first present the results of the reference simulation of a 50 m thick, impermeable sill emplaced at 3 km depth. Figure 6 displays the evolution of temperature, vitrinite reflectance (Ro) as a proxy for thermal maturity, permeability and methane concentrations in the model 1, 64 and 1000 years after the sill is emplaced. In the first few years after emplacement (left column in Figure 6), the sill is still over 1000°C hot and only the host rock very close to the sill is heated to temperatures of >350°C. Within the thin, barely visible thermal aureole, thermal maturity increases strongly and mineral dehydration takes place. In the dehydrated area, permeability increases from initial values of around 10^{-16} to 10^{-15} m^2 (Figure 6g). Figure 6g also shows a wider area of increased permeability indicated by the white dotted outline, which corresponds to the extent of hydrofracturing. The organic matter in the shale close to the contact shows a strong initial methane release, which travels toward the tip, where a small initial methane plume rises above the intrusion (Figure 6j).

After 64 years (central column in Figure 6), the high-temperature aureole in the surrounding host rock has expanded as the sill progressively cools down (Figure 6b). Within a distance of about 50 m around the sill, thermal maturity has reached Ro values above 2, which indicates the gas window or overmaturity (Figure 6e). Permeability in the same region is visibly elevated because the clay minerals are partly or fully dehydrated (Figure 6h). However, no more hydrofracturing occurs, since overpressures have dissipated and no longer exceed the tensile failure criterion. Methane concentrations now show a wide plume of methane rising on top of the sill and especially over its tip, but also a sizable accumulation remaining below the sill (Figure 6k).

The right column in Figure 6 represents the end of the simulation after 1000 years. The temperatures throughout the model are still elevated with respect to the initial geotherm but are now below 200°C everywhere. The dehydration-related permeability increase has not expanded significantly, but a second plume of very high methane concentrations is rising above the sill, but at some distance to its tip. The peak of the first plume has reached ca. 300

https://doi.org/10.5194/egusphere-2022-987
Preprint. Discussion started: 10 October 2022

372 m above the sill at this point. The aureole below the sill has also accumulated high methane
373 concentration of up to 800 kg per m^3 of water, which remain trapped below the impermeable
374 sill.

375

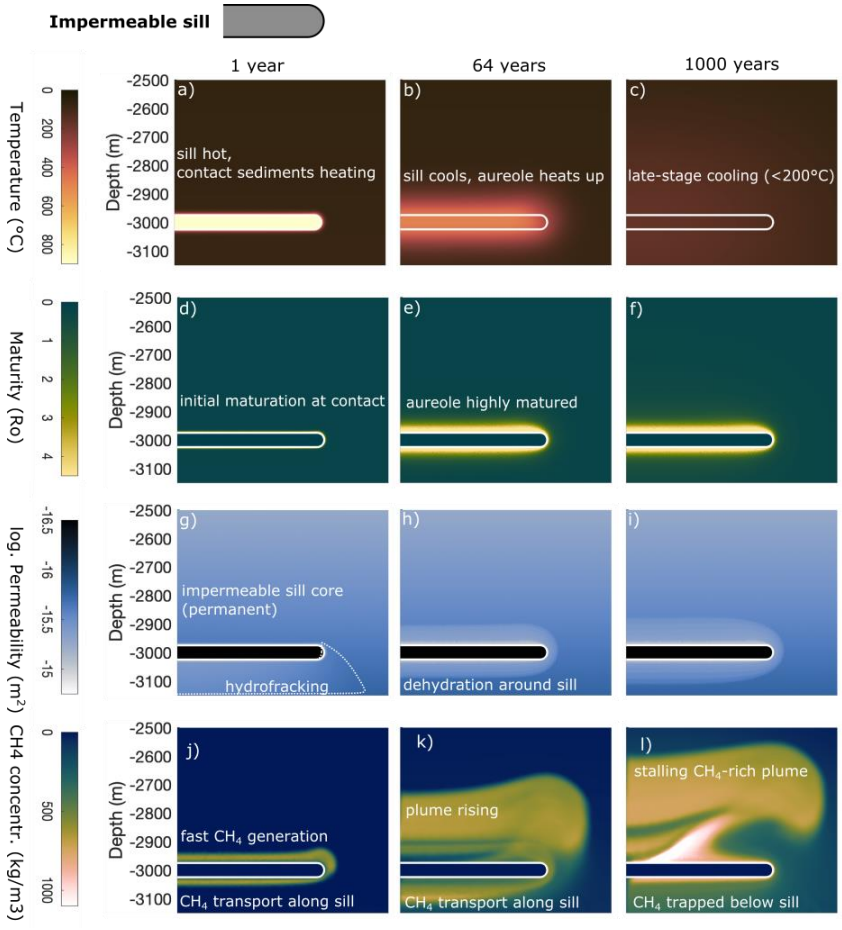

Figure 6. Reference simulation results for an impermeable sill of 50 m thickness at 3 km depth. The columns correspond to 1, 64 and 1000 years of simulated time after emplacement, respectively. The rows represent four parameters characterizing thermal state, contact metamorphism and hydrothermal transport of methane: (a-c) Temperature, (d-f) thermal maturity / organic matter transformation as vitrinite reflectance Ro, (g-i) permeability, (j-l) methane concentration.

376 3.5.2 Permeable sill: Pressure release and flow reversal

377 The introduction of cooling-related permeability generation in the sill profoundly changes the
378 development of hydrothermal flow and methane transport patterns. We show identical

https://doi.org/10.5194/egusphere-2022-987
Preprint. Discussion started: 10 October 2022

parameters and time steps as for the reference simulations, i.e. temperature, vitrinite reflectance (thermal maturity), permeability and methane concentrations in the model area around the permeable sill (Figure 7). To describe the details of the evolving flow patterns, we add close-up figures for methane concentration and flow velocities displaying flow vectors as well as the accumulation of methane and average temperature in the permeable and porous sill (Figure 8).

In the early phase, initial cooling of the sill leads to a progressing permeability front where the temperatures approach the solidus defined as 900°C. At this stage, the simulation closely resembles the reference run (Figure 7, left column). Temperatures in the sediments are elevated only very close to the intrusion, where the sediments almost instantly produce gas or become thermally overmature, i.e. vitrinite reflectance is larger than 1.5 (Figure 7a, d). Permeability in the sediments increases due to dehydration near the intrusion contact and hydrofracturing in the area within the dotted line below the sill (Figure 7g). Although large-scale methane concentrations appear nearly identical to the reference scenario, the detailed view shows that the onset of porosity and permeability generation in the sill's outermost regions allows some limited methane transport into the sill (Figure 8a.1). Nevertheless, most fluid flow and methane transport occur parallel to the sill contact and only rise upward around the sill tip (Figure 8a.1, a.4). Since methane generation in the aureole continues but transport is directed sideways within the host rock, the fraction of methane stored in the sill itself reduces (Figure 8b).

However, after the entire sill has become fully permeable, the flow direction along the sill center suddenly changes from horizontal, contact-parallel to near-vertical (Figure 7h, k, Figure 8a.2, a.5). The hydrothermal fluids transport the high methane concentrations from the lower aureole directly through the sill and into the upper aureole (Figure 7h, Figure 8a.2). In the upper aureole temperatures and thermal maturity are now higher than in the lower aureole (Figure 7b, e). At the same time, the flow directions at the intrusion tip also change and a circular flow pattern develops centered around a vortex located at the top of the intrusion tip (Figure 8a.2, a.5). This vortex initiates a downward directed flow that transports some of the methane from the flat rising plume above the sill back towards and into the sill tip (Figure 7k). During this phase of "methane flushing", more methane enters the sill from below and through the tip than is lost through the top contact, and thus both absolute and fractional methane stored in the intrusion rises until ca. 90 years of simulation (Figure 8b). Interestingly, the average temperature in the sill during this stage is still between 400-800°C (Figure 8b). The flow of

https://doi.org/10.5194/egusphere-2022-987
Preprint. Discussion started: 10 October 2022

fluids through the sill also leads to an increased cooling rate from the moment when the sill becomes fully permeable, as is indicated by the "kink" of the temperature curve at ca. 20 years (Figure 8b). Note also that the flow velocities drop by about 2 orders of magnitude compared to the initial years and are now on the order of 10 cm/year after 64 years of simulation.

In the following phase until the end of the simulation, the sill and sediments cool down to below 200°C, and thermal maturity and permeability only increase marginally (Figure 7c, f, i). The release of methane previously trapped under the sill creates a slowly rising band of very high methane concentrations above the sill (Figure 7l). At the tip, continuous circular flow creates a spatially confined area of very high methane concentration (Figure 8a.3, a.6). However, flow velocities have further reduced by another 2 orders of magnitude (Figure 8a.6). Overall, the sill maintains the total amount of stored methane due to approximately equal inflow and outflow (Figure 8b). However, since methane generation continues in the shale, the fraction of total methane stored in the sill reduces to ca. 5% from 500 years of simulation and onwards.

In summary, we identify three hydrothermal flow phases in the case of a sill with permeability evolution due to cooling joints. These include (i) pre-fracturing contact-parallel flow and methane transport, (ii) post fracturing methane-flushing and partial backflow and (iii) stabilization of methane in sill and late-stage methane generation.

https://doi.org/10.5194/egusphere-2022-987
Preprint. Discussion started: 10 October 2022

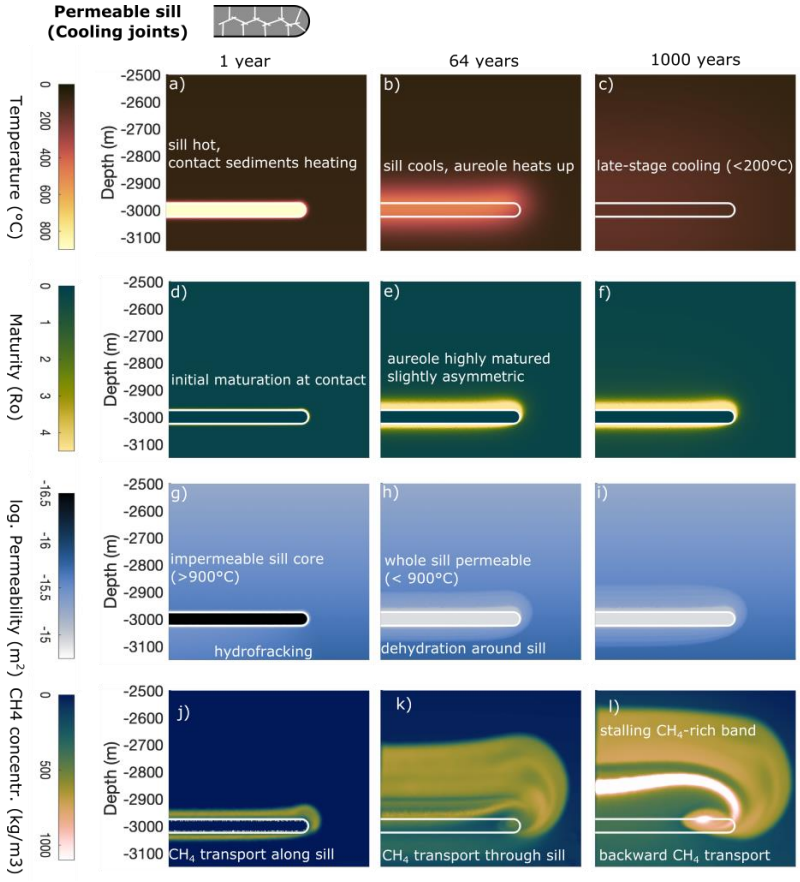

Figure 7. Simulation results for identical conditions as the reference case in Figure 6 (50 m thick, 3 km depth), but the sill develops porosity and permeability with cooling. The columns correspond to 1, 64 and 1000 years of simulated time after emplacement, respectively. The rows represent four parameters characterizing thermal state, contact metamorphism and hydrothermal transport of methane: (a-c) Temperature, (d-f) thermal maturity / organic matter transformation as vitrinite reflectance Ro, (g-i) permeability, (j-l) methane concentration.

https://doi.org/10.5194/egusphere-2022-987
Preprint. Discussion started: 10 October 2022

433

434

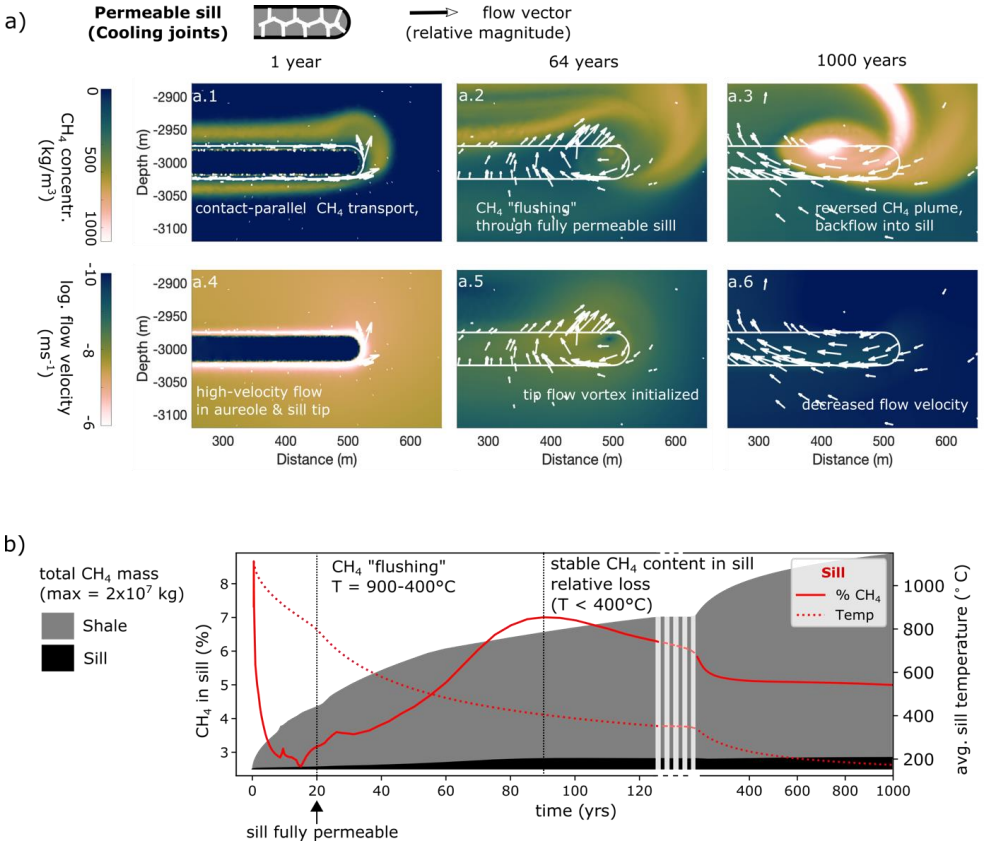

Figure 8. (a.1-a.6) Detailed view of the simulation of a permeable sill (50 m thick, 3 km depth, cf. Figure 7). The columns correspond to 1, 64 and 1000 years after emplacement, respectively. The rows show methane concentration (a.1-a.3) and flow velocity (a.4-a.6). The arrows represent flow vectors, with length differences representing relative magnitudes. Note that irregular arrow spacing is due to increased mesh fineness in and around the sill. (b) Fraction of total methane stored in the sill (solid line) and average temperature inside the sill (dotted line) throughout the simulation displayed above. Note that x-axis scaling is changed after 125 years, as indicated visually.

435

436

437

438

439

https://doi.org/10.5194/egusphere-2022-987
Preprint. Discussion started: 10 October 2022

3.5.3 Effects of emplacement depth and sill thickness

Finally, we explore the influence of emplacement depth and sill thickness on the resulting hydrothermal flow and methane transport pattern in case of a permeable sill (Figure 9). Not surprisingly, deeper and larger sills lead to more methane generation, but the transport of methane differs significantly because the flow patterns are affected in several ways. First, backward flow toward the intrusions similar to that described in the former section occurs only for deep emplacement depths, i.e. generally low permeability of the host rock due to burial, and for relatively thick intrusions (Figure 9a, d, g). In contrast, very thin intrusions (10 m) mainly generate a thick band of rising methane but little to no backflows at this depth (Figure 9f, i).

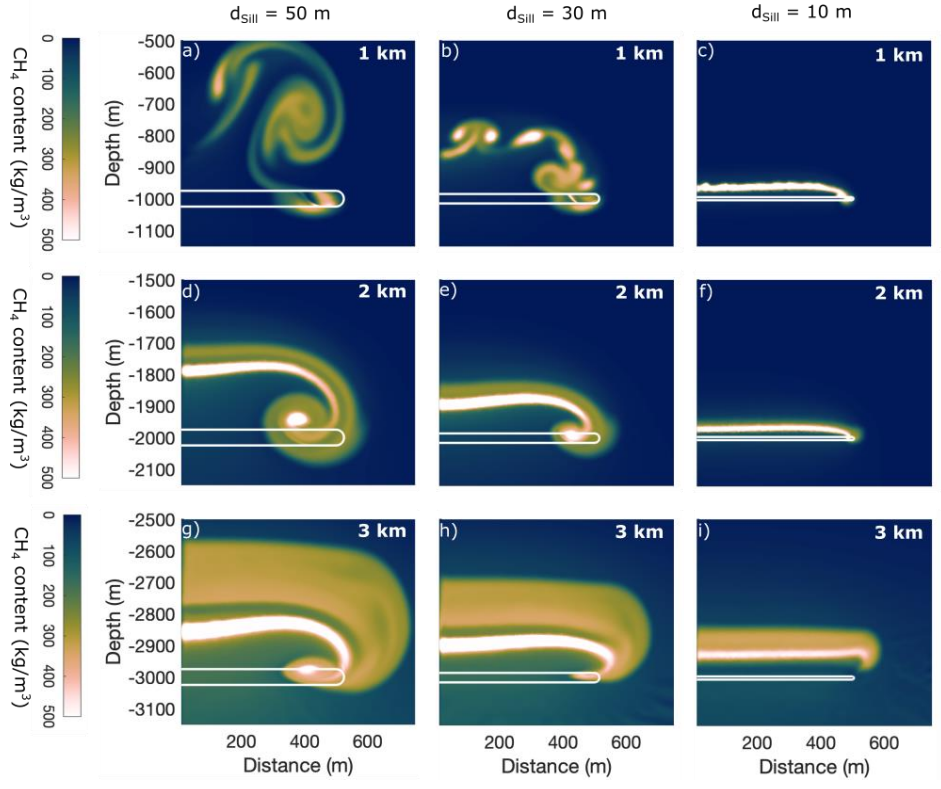

Figure 9. Parameter study results for the effect of varying emplacement depths and sill thicknesses on the final methane distribution after 1000 years, assuming a permeable sill. The columns represent different thicknesses of 50 m, 30 m and 10 m, respectively. The rows show emplacement depths of 1 km, 2 km, and 3 km, respectively, and thus include associated changes in host rock porosity and permeability as displayed in Figure 2b.

https://doi.org/10.5194/egusphere-2022-987
Preprint. Discussion started: 10 October 2022

At 1km depth, however, the characteristics of the hydrothermal flow patterns change drastically. Although some methane remains inside and below the sill tip, the backflow around a tip-vortex is no longer the dominant feature. Instead, hydrothermal convection cells develop above the intrusion and a methane plume rises towards the surface (Figure 9a,b). After 1000 years, the plume generated by the 50 m thick sill has risen by 500m, which is more than double compared to the 30 m thick sill at the same depth, or a 50 m thick sill at 2 km depth (Figure 9a, b, d).

4 Interpretation and discussion

4.1 Hydrocarbon transport through hot sills

Outcrop data strongly suggests that transport of hydrocarbons generated around the sills in the northern Neuquén Basin occurs both vertically through the igneous intrusions as well as around their tip. Importantly, geochemical data from the study area suggests that the sills are responsible for most, if not all, organic matter transformation in the host rock, because background maturity between the sills is essentially zero (Spacapan et al., 2018; Rabbel et al., 2021). We thus interpret the observed hydrocarbons in the field to result from magmatic and hydrothermal activity rather than burial-related maturation.

Cooling joints and veins or dykes filled with black shale and bitumen are pervasive throughout the fracture networks of sills in our study area (Figure 2 and Figure 3). The example shown in Figure 2 is particularly clear in showing the relationship between upwelling fluidized structures and the fill of the cooling joints. Note that similar observations have been documented in other outcrops at larger scales (Rabbel et al., 2021). We therefore propose that the flow of hot fluids and fluidized sediments through sills is a common occurrence in the northern Neuquén Basin. We thus provide solid outcrop evidence that sills can become a preferred hydrocarbon transport pathways upon cooling. In contrast, this finding contradicts the widespread assumption of impermeable intrusions in modeling studies of hydrothermal fluid flow in volcanic basins (e.g., Iyer et al., 2013; Iyer et al., 2017; Galerne and Hasenclever, 2019).

Our observations complement numerous growing evidence of hydrocarbons or fluidized sediments within sills of widely different sizes exist for instance in the Faroe-Shetland Basin (Rateau et al., 2013; Schofield et al., 2020), Karoo Basin (Svensen et al., 2010) and Guyamas

https://doi.org/10.5194/egusphere-2022-987
Preprint. Discussion started: 10 October 2022

Basin (Teske et al., 2021). Svensen et al. (2010) found metamorphosed sandstone dykes within dolerite sills in the Karoo Basin with mineral assemblage indicative of temperatures >300°C. They proposed that strong pressure gradients between the overpressured host rocks and the solidifying and contracting sill intrusions are likely responsible for liquefied sediments entering the intrusions shortly after cooling. Similar to this study, Svensen et al. (2010) based this interpretation on coupled thermo-hydraulic models, but explicitly considered thermal contraction of the magma. Although our approach of adding porosity to the sill is a simplification of this process, the general mechanism of hydrocarbon-rich fluids and sediments entering the cooling joint network in the intrusions in the Neuquén Basin is similar. We thus infer that our observations of hydrocarbon flow through hot sills in the Neuquén Basin are widespread in volcanic basins worldwide.

4.2 Impact of permeable sills on hydrothermal flow

Our numerical simulations allow us to assess the effects of implementing porosity and permeability increase due to fracturing when the sill has reached the solidus temperature. In simulations with an impermeable (i.e., unfractured) sill, the intrusion acts as a constant barrier for the hydrothermal flow and methane transport, and only the aureole shows permeability evolution due to fracturing and dehydration (Figure 6a, d, g). In this configuration, a upward-rising methane plume initiates from the top contact of the sill. In addition, large amounts of methane are trapped below the sill, since no vertical pathways are available through the sill (Figure 6g, j).

In contrast, a permeable sill introduces drastic changes in the flow and methane transport patterns, and results in three distinct phases with very different characteristics.

Phase 1: Impermeable sill and contact-parallel flow. Prior to complete solidification, the sill acts as a flow boundary and the flow patterns are essentially the same as in the reference simulation, i.e., rising methane above the sill and contact-parallel flow and extensive hydrofracturing below the sill (Figure 6g, j; Figure 7g, j, Figure 8a.1, a.4). Hydraulic fractures in the aureole and around the sill edge initiate in this early phase, which may lead to the formation of the large bitumen dykes and calcite veins observed in the field (Figure 3).

Phase 2: Hydrothermal "flushing" through solidified, permeable sill. The generation of cooling-related porosity and permeability inside the sill initiates the abrupt change from

https://doi.org/10.5194/egusphere-2022-987
Preprint. Discussion started: 10 October 2022

contact-parallel flow towards the intrusion tip to vertical uprising through the sill (second column of Figure 7, Figure 8a.2, a.5). This effect is responsible for a rush of hydrocarbon (here: methane) -rich fluids through the sill at average temperatures of 400-800°C (Figure 8b), because the large overpressure below the sills can now drive fluid flow straight upwards and dissipate instead of supplying a steady flow toward the sill tip. In addition, porosity generation inside the sill creates a suction effect that drives fluids into the intrusion (cf. Svensen et al., 2010). Considering flow velocities after 64 years (Figure 8a.2, a.5), the model shows that fluids flowing through a 50 m thick sill are exposed to this environment for tens of years, which could be sufficient for graphite generation and therefore seems to fit well with outcrop data and models for hydrothermal graphite generation (Figure 4; Rumble, 2014).

Phase 3: Vortex phase and reversed flow. The sudden change in the pore pressure distribution due to permeability creation within the sill also initiates the vortex observed above the sill tip and leads to the observed flow reversal and methane transport towards the sill tip (right column Figure 7; Figure 8a.3, a.6). However, in the long run the amount of methane influx toward the sill approximately equals the loss through upward flow so that the amount of methane is stable within the sill, and the fraction of total methane stored in the sill reduces after the "flushing" phase (Figure 8b). Hydrocarbons entering the sill in this last phase does not experience the extreme temperatures and have better chances of survival.

4.3 Impact of depth and thickness of permeable sills on hydrothermal flow

The first two phases, i.e. contact-parallel flow followed by methane "flushing", occur in all simulations with permeability creation within the cooling sill in a very similar fashion, which fits well with the fact that we observe graphitic material in sills of all sizes in the field. However, the final flow configuration and methane distribution shows important differences with intrusion thickness and emplacement depth (Figure 9). At depths of at least 2 km, i.e., emplacement depths approximately corresponding to the Agrio and Vaca Muerta formations in the study area, the dominant feature is the backflow at the sill tip from an otherwise evenly rising band of very high methane concentration (Figure 9d, g). Conversely, for the shallowest case (1 km), higher background permeability now allows the formation of large convection cells that transport methane towards the surface, while accumulation in the sill itself is very limited (Figure 9a). Thus, shallow permeable sills seem to favour hydrothermal upward transport of methane. This conclusion corresponds well with the results of Iyer et al. (2013) who found that in shallow, high permeability settings, release of fluids through permeable

https://doi.org/10.5194/egusphere-2022-987
Preprint. Discussion started: 10 October 2022

sills could be an important factor for greenhouse gas emissions from contact aureoles of sill intrusions.

Furthermore, the thinnest sills modelled do not have sufficient thermal energy to create the required pressure anomaly to sustain a flow vortex and backward flow of methane similar to the larger intrusions (Figure 9c, f, i). This is especially true for the deeper intrusions, where lower permeability of the host rock generally inhibits fluid flow. Since most of the sills emplaced in our study area are less than 30 m thick, we expect that only few sills create significant backflow.

4.4 Implications for fluid flow and methane transport

The strong contrast between the simulations with permeable and impermeable sills has important implications for the understanding of hydrothermal flow in volcanic basins, and notably on the formation of hydrothermal vent complexes and gas release to the atmosphere. Permeable sills strongly favor upward vertical flow and fluid pressure dissipation, especially in low-permeability host rocks, whereas impermeable sills favor fluid pressure build-up and contact-parallel flow towards sill tips. These latter mechanisms are the main responsible for the formation of hydrothermal vent complexes at sill tips (Iyer et al., 2017; Galerne and Hasenclever, 2019). Conversely, since the opening of vertical pathways through the sills due to cooling joints efficiently dissipates overpressure, permeable sills could potentially inhibit vent formation, or at least reduce atmospheric degassing.

Although we do not attempt to model vent formation here, our study can serve as a starting point to investigate the favorable conditions for hydrothermal vent formation. Our findings suggest that imposing impermeable sills in hydrothermal models is a strong assumption that may artificially ease the formation of hydrothermal vent complexes. Although there are good arguments to assume that massive, unfractured and impermeable intrusions dominate in many volcanic basins, the growing evidence of permeable sills during cooling (see section 6.1) suggests that this assumption should be critically evaluated on a case-by-case basis, and might explain the lack of hydrothermal vent complexes in some volcanic basins, like in the Neuquén Basin. We argue that future hydrothermal modelling studies of intrusion in sedimentary basins need to include sound justification for the chosen permeability and porosity evolution of the sills.

Additionally, the occurrence of graphitic bitumen in dykes and as filling of cooling joints indicates that part of the carbon gases rising through permeable sills could be reduced to

https://doi.org/10.5194/egusphere-2022-987
Preprint. Discussion started: 10 October 2022

graphite and be stored as solids (Figure 2, Figure 3, Figure 4). This fraction of carbon is strapped permanently underground and is not available for degassing in the atmosphere. The widespread observations of graphite in the field suggests that a significant fraction of hydrocarbons maturated in the sills metamorphic aureoles may not be mobilized. Currently, the fraction of methane transformed to immobile graphite, and so how much this reduced methane transport, is not known.

4.5 Implications for igneous petroleum systems in the Río Grande Valley

Our study also provides further insight into the evolution of the igneous petroleum systems in the Río Grande Valley, in particular with respect to the timing of the charging of the igneous hydrocarbon reservoirs. The current conceptual models comprise three main phases after sill emplacement into the previously immature shale formations (Witte et al., 2012; Spacapan et al., 2018; Spacapan et al., 2020). During the initial "thermal stage", the heat input from the sills generates liquid and gaseous hydrocarbons. During the second so-called "cooling stage", hydrocarbons hydrothermally migrate into the sill once cooling joints form. The last stage comprises tectonic fracturing and late-stage migration of hydrocarbons into the sills.

In this model, a significant part of the producible hydrocarbons migrates into the sill during the cooling stage, after the formation of colling joints. However, our study shows that hydrocarbons indeed migrate into the intrusions when the cooling joint network has formed, but experience far too high temperatures (at least 400°C) for them to survive as producible liquids or gases. In addition, regardless the scenarios tested in our simulations, temperatures during the main phase of accumulation of hydrocarbons in the intrusion still exceed 300°C (Figure 8b). Therefore, a survival of hydrocarbons entering the cooling joint network shortly after its creation seems highly unlikely. This result suggests that the charging of the igneous reservoirs occurs during the late-stage cooling of the sills, and after significant amounts of hydrocarbons has flowed through the sills at high temperature. The cooling stage of the models proposed earlier thus needs to be revised and split into two sub-stages: (1) a first influx of hydrocarbons through still hot sills, with no survival hydrocarbons, and (2) a later migration of hydrocarbons within the cooled sill, where the hydrocarbons can survive and be trapped to form producible reservoirs.

https://doi.org/10.5194/egusphere-2022-987
Preprint. Discussion started: 10 October 2022

4.6 Study limitations and future recommendations

Finally, we present selected recommendations for future work arising from the limitations of our study. Despite the complexity of the current numerical model, some known processes are not yet considered. First, mineral precipitation at high temperatures can occur at non-negligible rates and lead to fast porosity-decrease, causing pore pressure increase and possibly fracturing (Townsend, 2018). Fracturing in the aureole may not be reversible but permanently increase porosity and permeability, which has been documented in systematic core studies of contact aureoles in the RGV (Spacapan et al., 2019). These features should be included in future research, and the model predictions tested against field and laboratory studies. Finally, due to the strong effect on hydrothermal flow, it is critical to investigate under which circumstances cooling joints, which exist in many sheet intrusions, become available flow pathways.

5 Conclusions

In this study, we integrate geological field data with numerical models to investigate hydrothermal transport of hydrocarbon-rich fluids around fractured igneous sills. We use outcrops of fractured sills emplaced in organic-rich shales in the northern Neuquén Basin to establish that sills can become permeable fluid pathways upon solidification, which affects the fate of locally generated hydrocarbons. The numerical modelling study allows us to understand the main phases of hydrothermal flow and the kilometre-scale flow patterns in response to porosity and permeability generation inside a sill intrusion. This provides new insights into hydrothermal flow in volcanic sedimentary basins, because previous studies commonly assume that sills represent permanently impermeable bodies. The main conclusions of this study are as follows:

1. Widespread occurrence of veins with solid, strongly graphitized bitumen as well as cooling joints filled with solid bitumen or organic-rich shales evidence transport of hydrocarbon-rich fluids and liquefied sediments into the sill in a high-temperature (probably >350°C), high-pressure environment.

https://doi.org/10.5194/egusphere-2022-987
Preprint. Discussion started: 10 October 2022

2. Numerical modelling indicates three distinct flow phases around sills that become porous and permeable upon solidification, which affects transport of hydrocarbons generated in the contact aureole:

    (1) Contact-parallel flow toward the tip prior to solidification, creating an early plume above the sill tip

    (2) Sudden change to vertical flow upon complete solidification and "flushing" of hydrocarbons from the lower contact aureole upwards through the sill. This almost instantly dissipates much of the overpressure below the sill.

    (3) "Post-flushing" flow regime with slow rise of hydrocarbon-rich fluids above the sill center, and backward-downward flow towards the sill tip due to a vortex initialized by the sudden pressure reconfiguration

3. Simulations indicate that "flushing" of methane through the sill occurs at temperatures >400°C, which meets the conditions for hydrothermal graphitization. This may explain field observations of graphitic bitumen dykes.

4. Migration via reverse flow through a tip vortex during the post-flushing phase is very limited or absent for thin sills (< 30m) in low-permeable host rocks, which applies to many sill in the study area.

5. Permeability creation with the cooling sills may considerably reduce pressure build-up below the sills, and thus reduce the potential for hydrothermal venting. With growing evidence for permeable sills in volcanic basins globally, the permeability evolution of sills should be addressed in future modelling studies focused on sill-related venting.

6. In contrast to proposed conceptual models, flow of hydrocarbons into newly formed cooling joints is likely not a viable migration mechanism for igneous sill reservoirs in the northern Neuquén Basin, as the intrusions are too hot for survival of liquid hydrocarbons.

https://doi.org/10.5194/egusphere-2022-987
Preprint. Discussion started: 10 October 2022

Acknowledgements

Rabbel's position was funded by the Faculty of Mathematics and Natural Science of the University of Oslo, through the "Earth Flows" Strategic Initiative project. The DEEP Research School provided funding for fieldwork (249040/F60).

References

Aarnes, I., Podladchikov, Y.Y., Svensen, H., 2012. Devolatilization-induced pressure build-up: Implications for reaction front movement and breccia pipe formation. Geofluids 12, 265-279, 10.1111/j.1468-8123.2012.00368.x.

Aarnes, I., Svensen, H., Connolly, J.A.D., Podladchikov, Y.Y., 2010. How contact metamorphism can trigger global climate changes: Modeling gas generation around igneous sills in sedimentary basins. Geochimica et Cosmochimica Acta 74, 7179-7195, http://dx.doi.org/10.1016/j.gca.2010.09.011.

Angenheister, G., Cermak, V., Huckenholz, H., Rybach, L., Schmid, R., Schopper, J., Schuch, M., Stoeffler, D., Wohlenberg, J., 1982. Physical properties of rocks. Subvol. a.

Beyssac, O., Goffé, B., Chopin, C., Rouzaud, J.N., 2002. Raman spectra of carbonaceous material in metasediments: a new geothermometer. Journal of Metamorphic Geology 20, 859-871, 10.1046/j.1525-1314.2002.00408.x.

Buseck, P.R., Beyssac, O., 2014. From organic matter to graphite: Graphitization. Elements 10, 421-426.

Chevallier, L., Gibson, L.A., HNhleko, L.O., Woodford, A.C., Nomquphu, W., Kippie, I., 2004. Hydrogeology of fractured-rock aquifers and related ecosystems within the Qoqodala dolerite ring and sill complex, Great Kei catchment, Eastern Cape, Water Res. Com., S. Afr., p. 127.

Cobbold, P.R., Diraison, M., Rossello, E.A., 1999. Bitumen veins and Eocene transpression, Neuquén basin, Argentina. Tectonophysics 314, 423-442.

Combina, A., Nullo, F., 2005. Tertiary volcanism and sedimentation in the southern Cordillera Principal, Mendoza, Argentina, in: Proceedings of the 6th International Symposium on Andean Geodynamics, Barcelona, Spain, 12-14 September 2005, 174-177.

Connolly, J., 2009. The geodynamic equation of state: what and how. Geochemistry, Geophysics, Geosystems 10.

Delaney, P.T., 1982. Rapid intrusion of magma into wet rock: Groundwater flow due to pore pressure increases. Journal of Geophysical Research: Solid Earth 87, 7739-7756.

https://doi.org/10.5194/egusphere-2022-987
Preprint. Discussion started: 10 October 2022

698 Einsele, G., Gieskes, J.M., Curray, J., Moore, D.M., Aguayo, E., Aubry, M.-P., Fornari, D., Guerrero,
699 J., Kastner, M., Kelts, K., Lyle, M., Matoba, Y., Molina-Cruz, A., Niemitz, J., Rueda, J.,
700 Saunders, A., Schrader, H., Simoneit, B., Vacquier, V., 1980. Intrusion of basaltic sills into
701 highly porous sediments, and resulting hydrothermal activity. Nature 283, 441-445, doi:
702 10.1038/283441a0.
703 Galerne, C.Y., Hasenclever, J., 2019. Distinct Degassing Pulses During Magma Invasion in the
704 Stratified Karoo Basin—New Insights From Hydrothermal Fluid Flow Modeling.
705 Geochemistry, Geophysics, Geosystems 20, 2955-2984, 10.1029/2018GC008120.
706 Hays, W.W., Nuttli, O.W., Scharon, L., 1967. Mapping gilsonite veins with the electrical resistivity
707 method. Geophysics 32, 302-310.
708 Hetényi, G., Taisne, B., Garel, F., Médard, É., Bosshard, S., Mattsson, H.B., 2012. Scales of columnar
709 jointing in igneous rocks: field measurements and controlling factors. Bulletin of
710 Volcanology 74, 457-482, 10.1007/s00445-011-0534-4.
711 Howell, J.A., Schwarz, E., Spalletti, L.A., Veiga, G.D., 2005. The Neuquén Basin: an overview, in:
712 Veiga, G.D., Spalletti, L.A., Howell, J.A., Schwarz, E. (Eds.), Geological Society, London,
713 Special Publications, 252, 1-14.
714 Iyer, K., Rüpke, L., Galerne, C.Y., 2013. Modeling fluid flow in sedimentary basins with sill
715 intrusions: Implications for hydrothermal venting and climate change. Geochemistry,
716 Geophysics, Geosystems 14, 5244-5262, 10.1002/2013GC005012.
717 Iyer, K., Schmid, D.W., Planke, S., Millett, J., 2017. Modelling hydrothermal venting in volcanic
718 sedimentary basins: Impact on hydrocarbon maturation and paleoclimate. Earth Planet. Sci.
719 Lett. 467, 30-42, https://doi.org/10.1016/j.epsl.2017.03.023.
720 Jamtveit, B., Svensen, H., Podladchikov, Y.Y., Planke, S., 2004. Hydrothermal vent complexes
721 associated with sill intrusions in sedimentary basins. Physical Geology of High-Level
722 Magmatic Systems. Geological Society, London, Special Publications 234, 233-241.
723 Kay, S.M., Burns, W.M., Copeland, P., Mancilla, O., 2006. Upper Cretaceous to Holocene
724 magmatism and evidence for transient Miocene shallowing of the Andean subduction zone
725 under the northern Neuquén Basin. Geological Society of America Special Papers 407, 19-60.
726 Kietzmann, D.A., Palma, R.M., Riccardi, A.C., Martín-Chivelet, J., López-Gómez, J., 2014.
727 Sedimentology and sequence stratigraphy of a Tithonian–Valanginian carbonate ramp (Vaca
728 Muerta Formation): a misunderstood exceptional source rock in the Southern Mendoza area
729 of the Neuquén Basin, Argentina. Sedimentary geology 302, 64-86.
730 Kobchenko, M., Hafver, A., Jettestuen, E., Renard, F., Galland, O., Jamtveit, B., Meakin, P.,
731 Dysthe, D. K., 2014. Evolution of a fracture network in an elastic medium with
732 internal fluid generation and expulsion. Physical Review E, 90(5), 052801.

https://doi.org/10.5194/egusphere-2022-987
Preprint. Discussion started: 10 October 2022

Kwiecinska, B., Suárez-Ruiz, I., Paluszkiewicz, C., Rodriques, S., 2010. Raman spectroscopy of selected carbonaceous samples. International Journal of Coal Geology 84, 206-212.

Manceda, R., Figueroa, D., 1995. Inversion of the Mesozoic Neuquén rift in the Malargüe fold and thrust belt, Mendoza, Argentina, in: Tankard, A.J., S., S., Welsink, H.J. (Eds.), Petroleum basins of South America: AAPG Memoir, 62, 369–382.

Mark, N., Schofield, N., Pugliese, S., Watson, D., Holford, S., Muirhead, D., Brown, R., Healy, D., 2018. Igneous intrusions in the Faroe Shetland basin and their implications for hydrocarbon exploration; new insights from well and seismic data. Marine and Petroleum Geology 92, 733-753.

Marsh, B.D., 2002. On bimodal differentiation by solidification front instability in basaltic magmas, part 1: basic mechanics. Geochimica et Cosmochimica Acta 66, 2211-2229, https://doi.org/10.1016/S0016-7037(02)00905-5.

Nermoen, A., Galland, O., Jettestuen, E., Fristad, K., Podladchikov, Y.Y., Svensen, H., Malthe-Sørenssen, A., 2010. Experimental and analytic modeling of piercement structures. J. Geophys. Res. 115, B10202, 10.1029/2010jb007583.

Palma, J.O., Spacapan, J.B., Rabbel, O., Galland, O., Ruiz, R., Leanza, H.A., 2019. The atypical igneous Petroleum System of the Cara Cura range, southern Mendoza province, Argentina, in: The Physical Geology of Subvolcanic Systems: Laccoliths, Sills and Dykes (LASI6), Malargüe, Germany, 25-29 November 2019, 159-161, 2019

Panahi, H., Kobchenko, M., Meakin, P., Dysthe, D.K., Renard, F., 2018. In-situ imaging of fracture development during maturation of an organic-rich shale: Effects of heating rate and confinement. Marine and Petroleum Geology 95, 314-327.

Petford, N., 2003. Controls on primary porosity and permeability development in igneous rocks. Hydrocarbons in Crystalline Rocks 214, 93-107.

Potgieter-Vermaak, S., Maledi, N., Wagner, N., Van Heerden, J., Van Grieken, R., Potgieter, J., 2011. Raman spectroscopy for the analysis of coal: a review. Journal of Raman Spectroscopy 42, 123-129.

Rabbel, O., 2017. Integrated Seismic and Rock Physics Modelling of Oil-Producing Volcanic Sills in the Neuquén Basin, Argentina, Department of Geosciences. University of Oslo, Oslo, p. 83.

Rabbel, O., Galland, O., Mair, K., Lecomte, I., Senger, K., Spacapan, J.B., Manceda, R., 2018. From field analogues to realistic seismic modelling: a case study of an oil-producing andesitic sill complex in the Neuquén Basin, Argentina. J. Geol. Soc., 10.1144/jgs2017-116.

Rabbel, O., Mair, K., Galland, O., Grühser, C., Meier, T., 2020. Numerical modeling of fracture network evolution in organic-rich shale with rapid internal fluid generation. Journal of Geophysical Research: Solid Earth 125, e2020JB019445.

https://doi.org/10.5194/egusphere-2022-987
Preprint. Discussion started: 10 October 2022

768 Rabbel, O., Palma, J.O., Mair, K., Galland, O., Spacapan, J.B., Senger, K., 2021. Fracture networks in
769 shale-hosted igneous intrusions: Processes, distribution and implications for igneous
770 petroleum systems. J. Struct. Geol. 150, 104403, https://doi.org/10.1016/j.jsg.2021.104403.
771 Rantitsch, G., Lämmerer, W., Fisslthaler, E., Mitsche, S., Kaltenböck, H., 2016. On the discrimination
772 of semi-graphite and graphite by Raman spectroscopy. International Journal of Coal Geology
773 159, 48-56.
774 Rateau, R., Schofield, N., Smith, M., 2013. The potential role of igneous intrusions on hydrocarbon
775 migration, West of Shetland. Petroleum Geoscience 19, 259-272, doi: 10.1144/petgeo2012-
776 035.
777 Rodriguez Monreal, F., Villar, H.J., Baudino, R., Delpino, D., Zencich, S., 2009. Modeling an
778 atypical petroleum system: A case study of hydrocarbon generation, migration and
779 accumulation related to igneous intrusions in the Neuquen Basin, Argentina. Marine and
780 Petroleum Geology 26, 590-605, doi: 10.1016/j.marpetgeo.2009.01.005.
781 Rumble, D., 2014. Hydrothermal graphitic carbon. Elements 10, 427-433.
782 Schiuma, M.F. Intrusivos del valle del Río Grande, provincia de Mendoza, su importancia como
783 productores de hidrocarburos, Ph.D. thesis, Universidad Nacional de La Plata, Argentina, 234
784 pp., 1994
785 Schofield, N., Holford, S., Edwards, A., Mark, N., Pugliese, S., 2020. Overpressure transmission
786 through interconnected igneous intrusions. AAPG Bulletin 104, 285-303.
787 Schön, J.H., 2015. Physical properties of rocks: Fundamentals and principles of petrophysics.
788 Elsevier.
789 Senger, K., Millett, J., Planke, S., Ogata, K., Eide, C., Festøy, M., Galland, O., Jerram, D.A., 2017.
790 Effects of igneous intrusions on the petroleum system: a review. First Break 35.6, 47-56,
791 10.3997/1365-2397.2017011.
792 Spacapan, J.B., D'Odorico, A., Palma, O., Galland, O., Rojas Vera, E., Ruiz, R., Leanza, H.A.,
793 Medialdea, A., Manceda, R., 2020. Igneous petroleum systems in the Malargüe fold and
794 thrust belt, Río Grande Valley area, Neuquén Basin, Argentina. Marine and Petroleum
795 Geology 111, 309-331, https://doi.org/10.1016/j.marpetgeo.2019.08.038.
796 Spacapan, J.B., D´Odorico, A., Palma, O., Galland, O., Senger, K., Ruiz, R., Manceda, R., Leanza,
797 H.A., 2019. Low resistivity zones at contacts of igneous intrusions emplaced in organic-rich
798 formations and their implications on fluid flow and petroleum systems: A case study in the
799 northern Neuquén Basin, Argentina. Basin Research, 10.1111/bre.12363.
800 Spacapan, J.B., Galland, O., Leanza, H.A., Planke, S., 2017. Igneous sill and finger emplacement
801 mechanism in shale-dominated formations: a field study at Cuesta del Chihuido, Neuquén
802 Basin, Argentina. J. Geol. Soc. 174, 422-433, 10.1144/jgs2016-056.
803 Spacapan, J.B., Palma, O., Galland, O., Manceda, R., Rocha, E., D'Odorico, A., Leanza, H.A., 2018.
804 Thermal impact of igneous sill complexes on organic-rich formations and the generation of a

https://doi.org/10.5194/egusphere-2022-987
Preprint. Discussion started: 10 October 2022

petroleum system: case study in the Neuquén Basin, Argentina. Mar. Pet. Geol. 91, 519-531, https://doi.org/10.1016/j.marpetgeo.2018.01.018.

Stern, C.R., Huang, W.-L., Wyllie, P.J., 1975. Basalt-andesite-rhyolite-H2O: Crystallization intervals with excess H2O and H2O-undersaturated liquidus surfaces to 35 kolbras, with implications for magma genesis. Earth and Planetary Science Letters 28, 189-196.

Svensen, H., Aarnes, I., Podladchikov, Y.Y., Jettestuen, E., Harstad, C.H., Planke, S., 2010. Sandstone dikes in dolerite sills: Evidence for high-pressure gradients and sediment mobilization during solidification of magmatic sheet intrusions in sedimentary basins. Geosphere 6, 211-224.

Svensen, H., Planke, S., Malthe-Sørenssen, A., Jamtveit, B., Myklebust, R., Rasmussen Eidem, T., Rey, S.S., 2004. Release of methane from a volcanic basin as a mechanism for initial Eocene global warming. Nature 429, 542-545, doi: 10.1038/nature02566.

Sweeney, J.J., Burnham, A.K., 1990. Evaluation of a simple model of vitrinite reflectance based on chemical kinetics. AAPG bulletin 74, 1559-1570.

Teske A, Lizarralde D, Höfig TW, and the Expedition 385 Scientists (2021): Expedition 385 Summary. Proceedings of the International Ocean Discovery Program 385. doi: 10.14379/iodp.proc.385.101.2021

Townsend, M.R., 2018. Modeling Thermal Pressurization Around Shallow Dikes Using Temperature-Dependent Hydraulic Properties: Implications for Deformation Around Intrusions. Journal of Geophysical Research: Solid Earth 123, 311-323.

Witte, J., Bonora, M., Carbone, C., Oncken, O., 2012. Fracture evolution in oil-producing sills of the Rio Grande Valley, northern Neuquen Basin, Argentina. AAPG Bulletin 96, 1253-1277, doi: 10.1306/10181110152.

Yagupsky, D.L., Cristallini, E.O., Fantín, J., Valcarce, G.Z., Bottesi, G., Varadé, R., 2008. Oblique half-graben inversion of the Mesozoic Neuquén Rift in the Malargüe Fold and Thrust Belt, Mendoza, Argentina: New insights from analogue models. Journal of Structural Geology 30, 839-853, https://doi.org/10.1016/j.jsg.2008.03.007.

Zanella, A., Cobbold, P.R., Ruffet, G., Leanza, H.A., 2015. Geological evidence for fluid overpressure, hydraulic fracturing and strong heating during maturation and migration of hydrocarbons in Mesozoic rocks of the northern Neuquén Basin, Mendoza Province, Argentina. J. S. Amer. Earth. Sci. 62, 229-242, http://dx.doi.org/10.1016/j.jsames.2015.06.006.